buildings

MDPI

Article

Strengthening Masonry Arches with Lime-Based Mortar Composite

Valerio Alecci [1,*], Mario De Stefano [1], Francesco Focacci [2], Raimondo Luciano [3], Luisa Rovero [1] and Gianfranco Stipo [1]

[1] Department of Architecture, University of Florence, piazza Brunelleschi 6, 50121 Firenze, Italy; mario.destefano@unifi.it (M.D.S.); luisa.rovero@unifi.it (L.R.); gianfranco.stipo@unifi.it (G.S.)
[2] eCampus University, via Isimbardi 10, Novedrate, 22060 Como, Italy; francesco.focacci@uniecampus.it
[3] Department of Mechanics, Structures and Environment, University of Cassino, via G. Di Biasio 43, 03043 Cassino, Italy; luciano@unicas.it
* Correspondence: valerio.alecci@unifi.it

Received: 13 April 2017; Accepted: 8 June 2017; Published: 13 June 2017

Abstract: In recent decades, many strengthening interventions on masonry elements were performed by using fiber reinforced polymers (FRPs). These advanced materials proved to be effective to increase the load-carrying capacity of masonry elements and to improve their structural behavior, avoiding the most critical failure modes. Despite the advantages of this technique compared to more traditional methods, FRP systems have disadvantages related to their low resistance to high temperatures, impossibility of application on wet surfaces, low permeability, and poor compatibility with masonry supports. Therefore, composite materials made of a fiber textile embedded in an inorganic matrix were recently proposed as alternatives to FRPs for strengthening historic masonry constructions. These composite materials are easier to install, have higher resistance to high temperatures, and permit higher vapor permeability than FRPs. The inorganic matrix is frequently a cement-based mortar, and the composite materials made of a fiber textile embedded in a cement-based mortar are usually identified as FRCM (fabric reinforced cementitious matrix) composites. More recently, the use of natural lime mortar as an inorganic matrix has been proposed as an alternative to cement-based mortars when historic compatibility with the substrate is strictly required, as in case of restoration of historic buildings. In this paper, the effectiveness of a fabric made of basalt fibers embedded in lime mortar matrix (Basalt-FRLM) for the strengthening of masonry arches is investigated. An experimental investigation was performed on 1:2 scaled brick masonry arches strengthened at the extrados with a layer of Basalt-FRLM and tested under vertical load. The results obtained are compared with previous results obtained by the authors by testing masonry arches strengthened at their extrados with FRCM and FRP composites. This investigation highlights the effectiveness of Basalt-FRLM in increasing load-currying and the displacement capacities of masonry arches. The Basalt-FRLM-strengthened arch exhibited higher displacement capacity when compared to arches strengthened with polymeric and cementitious matrix composites.

Keywords: masonry arch; strengthening; composite material; FRCM; lime mortar

1. Introduction

Masonry constructions are an important part of historical and artistic heritage. Recent seismic events have increased the attention of architects and engineers towards the assessment of the seismic response of historical buildings through more appropriate strategies, based on different approaches such as rocking analyses [1–6], energy-based methods [7], and numerical and experimental procedures [8–11].

Masonry arches and vaults are often present in historical buildings, representing elements of remarkable architectural value, but, at the same time, showing high seismic vulnerability. For this reason, there is an increasing interest in the development of innovative strengthening techniques to improve the structural performances of masonry arches and vaults. Traditional strengthening techniques (i.e., steel profiles or reinforced concrete hoods), which revealed many drawbacks, have been replaced by advanced strengthening solutions, based on the use of polymeric-based composite materials (fiber reinforced polymer, FRP). Innovative composite materials constituted by a fabric embedded in a cement-based matrix (FRCM, fabric reinforced cementitious mortar) are being studied [12–18] as an alternative to FRPs [19–23], mainly to strengthen historic buildings due to their high compatibility with masonry substrate in terms of resistance to high temperature and vapor permeability. Recently, a natural lime mortar matrix has been proposed as alternative to the cement-based matrix [24] when historic compatibility with the substrate is required, as in case of restorations of monumental buildings.

In this paper, the effectiveness of a composite material made of a basalt fiber textile embedded in a natural lime mortar (Basalt-FRLM) for strengthening masonry structures is investigated. In particular, the paper deals with an experimental campaign on brick masonry arches strengthened at the extrados with Basalt-FRLM. The structural behavior of Basalt-FRLM-strengthened arches is analyzed and compared with the structural behavior of un-strengthened arches and arches strengthened with FRP and FRCM composites tested in a previous step of this research [17,18,25]. The purpose of this research is to provide the first experimental evaluation of the structural effectiveness of lime matrix composite materials for strengthening masonry structures, and to compare it with the effectiveness which can be achieved with more traditional composite materials such as FRPs and FRCMs.

2. Experimental Program

An experimental campaign was performed on un-strengthened and extrados-strengthened models of brick masonry arches, in a scale of 1:2, subjected to a vertical force. The mechanical properties of the masonry components, cement-lime mortar, and bricks were obtained according to References [26,27], respectively. The masonry mechanical properties were evaluated with compressive tests on six masonry prisms in a scale of 1:2. Table 1 summarizes the mechanical properties of the masonry and its components.

Table 1. Results of tests performed on bricks, cement-lime mortar, and masonry (standard deviation and coefficient of variation are reported in parentheses). ε_u = failure strain; f_c = compressive strength; E_c = compressive Young modulus; f_{tf} = tensile flexural strength.

Material	ε_u	f_c [MPa]	E_c [MPa]	f_{tf} [MPa]
Cement-lime mortar	/	3.22 (0.31; 9.72)	727.7 (69.82; 9.59)	1.49 (0.025;1.68)
Brick	/	24.08 (2.73; 11.37)	2701.81 (585.05; 21.65)	5.60 (0.58; 10.44)
Masonry	0.0076 (0.002; 17.66)	8.53 (1.29; 13.95)	1753.7 (282.52; 16.11)	/

The Basalt-FRLM strengthening system used in this experimental investigation, produced by KeraKoll S.p.A (Sassuolo, Modena, Italy), is made up of a basalt bidirectional balanced textile (Figure 1a), named GeoSteel Grid 200, embedded in an Natural Hydraulic Limes (NHL) 3.5 lime mortar named GeoCalce® Fino (Sassuolo, Modena, Italy). The basalt fibers are provided with an alkali-resistant protective treatment made of solvent-free water-based resin and AISI 304 stainless steel micro-threads welded together to guarantee a stable sheet. The textile is made of 17-mm spaced rovings. Its equivalent thickness in both fiber directions is equal to 0.032 mm. The matrix has compressive

strength class M15 in agreement with EN 998-2. This mortar contains strictly raw, natural, and recycled minerals, with low CO_2 emissions material and very low emissions of volatile organic compounds. It is recycled as inert at the end of its life. The properties of basalt fibers and natural lime mortar are summarized in Table 2.

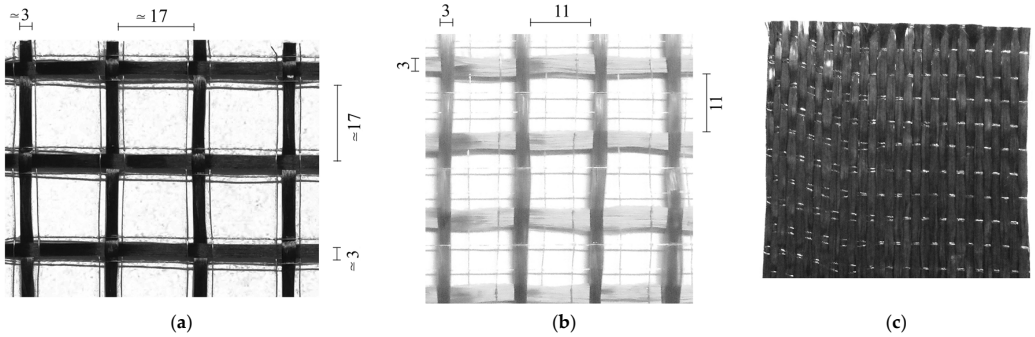

(**a**) (**b**) (**c**)

Figure 1. (**a**) Poliparafenilenbenzobisoxazole (PBO) balanced textile; (**b**) basalt balanced textile; (**c**) unidirectional carbon sheet. Dimensions in mm.

Table 2. Properties of the composite materials provided by the manufacturer. t_f = equivalent thickness; f_f = fiber tensile strength; E_f = fiber Young modulus; ε_{fu} = fiber failure strain f_{mc} = compressive strength; E_m = matrix Young modulus; f_{mtf} = tensile flexural strength. (*) Experimentally determined.

Composite Material	Fibers Material	t_f [mm]	f_f [MPa]	E_f [GPa]	ε_{fu} [%]	Matrix Material	f_{mc} [MPa]	E_m [GPa]	f_{mtf} [MPa]
Basalt-FRLM	Basalt	0.032	≥3000	≥87	-	Lime	11.2 (*)	1.3 (*)	3.72 (*)
PBO-FRCM	PBO	0.014	5800	270	2.5	Cement	20 (*)	2.8 (*)	6.15 (*)
CFRP	Carbon	0.17	4800	240	2.00	Epoxy	>50	-	-

An FRCM composite and an FRP composite produced by Ruredil S.p.A Company (San Donato Milanese, Milano, Italy) were also considered in this experimental investigation for comparison purposes. The FRCM composite, Ruregold® (San Donato Milanese, Milano) XR Muratura, is made up of a poliparafenilenbenzobisoxazole (PBO) fiber bidirectional balanced textile (Figure 1b) made of 14-mm spaced rovings (equivalent thickness 0.014 mm) embedded in a pozzolanic cement-based mortar. The FRP composite, Ruredil X Wrap 310, is made up of a unidirectional carbon sheet with an equivalent thickness 0.17 mm (Figure 1c), impregnated and glued to the substrate through a two-component epoxy-based matrix. These composites are denoted as PBO-FRCM and CFRP, respectively. Their properties are summarized in Table 2.

Experimental tests were carried out on five 1:2 scaled masonry arch models. The arch models had a 1500 mm span, 866 mm intrados radius, 961 mm extrados radius, 432.5 mm rise, and 95 mm × 95 mm cross-section (Figure 2). The dimensions of the bricks and the thickness of the mortar layers were scaled according to the scale of the model. Bricks had dimensions of 95 mm × 46 mm × 21 mm and were obtained by cutting standard bricks my means of a circular saw with water. The mortar joints were 5 mm thick. To obtain proper masonry mechanical properties, the compressive tests on masonry prisms, whose results are summarized in Table 1, were performed on specimens made of scaled bricks and thickness of the mortar joints.

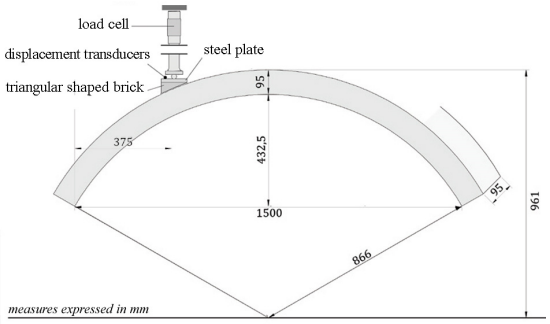

Figure 2. Scheme of the arch model test.

The choice to test 1:2 scaled models was decided by the limited dimension of the steel frame employed to perform the tests. It was impossible to scale the dimensions of the strengthening materials in terms of size of the mesh and size of the particles of the matrix, since commercial composites have been adopted in this study. Furthermore, the scaled models can be considered representative of masonry arches strengthened with two layers of textile. Two un-strengthened (specimens 1-US and 2-US) and three strengthened (specimens B-FRLM, P-FRCM, and CFRP) arches were tested. The adopted strengthening configuration consisted of the application of a layer of composite material on the whole extrados surface of the arches.

The compatibility between the masonry substrate and lime and cement matrices allowed their application without special treatments. After cleaning and damping the extrados surface, a first 3 mm thick layer of lime or cement matrix was applied. Subsequently, the textile was applied and finally another matrix layer of the same thickness was applied. For the CFRP composite, after cleaning the extrados surface, the classical hand layup procedure was applied; a thin layer of primer was applied prior to the application of the matrix. Subsequently, the epoxy matrix and the carbon sheet were applied. Finally, the composite material was completed with the application of a further layer of epoxy matrix.

Each arch was subjected to a vertical force applied at a quarter of the arch span (375 mm from one abutment, Figure 2). A displacement control device made of a screw jack controlled through a flywheel was used to register the loading history, up to the point of a conventional test-end corresponding to a residual strength equal to 80% of the maximum load. The load was measured through a load cell with a capacity of 100 kN (TCLP-10B tension/compression load cell). Two displacement transducers (type cantilever) were used to measure vertical displacements. The test apparatus and arch dimensions are represented in Figure 2.

3. Test Results

The experimental results are summarized in Table 3 in terms of failure load, tangent stiffness, kinematic ductility, and increase of failure load per unit cross-sectional area of fibers. The tangent stiffness is calculated as the slope of the linear phase of the load–displacement curve. The kinematic ductility is determined as the ratio of the displacement at the failure load to the displacement at the end of the linear phase of the load–displacement curve. The increase of the failure load per unit cross-sectional area of fibers is evaluated as:

$$\Delta f = \frac{F_{max} - F_{max0}}{A_f} \quad (1)$$

where F_{max} and F_{max0} are the failure loads of the strengthened and un-strengthened arches, respectively, and A_f is the cross-sectional area of the fibers in the composite material. Parameter Δf is representative of the strengthening effectiveness of the composite materials in terms of increase of failure load, while

kinematic ductility represents the capacity of the specimen to exhibit displacements after the linear elastic range, up to the peak load.

Table 3. Structural parameters identified during tests on arch models.

Specimen	Failure Load [N]	Tangent Stiffness [N/mm]	Kinematic Ductility	Δf [N/mm^2]
1-US	910	7179	1.85	-
2-US	1066	6197	1.11	-
Basalt-FRLM	5366	7200	36.6	1.37
PBO-FRCM	4968	16,221	20.32	2.84
CFRP	11,345	10,106	10.93	0.61

3.1. Un-Strengthened Arch Models

The un-strengthened arch models collapsed by the four-hinges mechanism, as shown in Figure 3. The first hinge (hinge 1) formed at the arch extrados on the loaded cross-section, while the second hinge (hinge 2) formed at the intrados. The third and fourth hinges (hinges 3 and 4) formed on the left and right abutment, respectively.

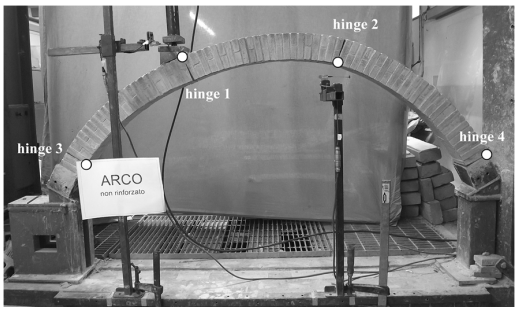

Figure 3. Hinges on the un-strengthened arches.

3.2. Arch Models Strengthened with Basalt-FRLM

The Basalt-FRLM-strengthened arch exhibited a different collapse mechanism, as shown in Figure 4. The first hinge (hinge 1) formed on the loaded cross-section, as it had happened in the un-strengthened arches. The opening of hinges 2 and 3 (Figure 3) was prevented by the composite material. A first crack was noted on the lime matrix, approximately where hinges 2 and 3 formed in the un-strengthened arch models. The onset of hinge 4 (Figure 3) occurred after the onset of hinge 1 and the cracking of the matrix, but it did not open due to the joint sliding at the right abutment of the arch. Before the collapse, additional cracks occurred on the lime mortar matrix near the cross-section where hinge 2 formed on the un-strengthened arches (Figure 5). The opening of these cracks was associated with slip of the fibers with respect to the surrounding matrix, and allowed a displacement capacity much higher than the displacement capacity of the un-strengthened arches. At the failure of the specimen, the lime mortar was still perfectly attached to the extrados of the arch.

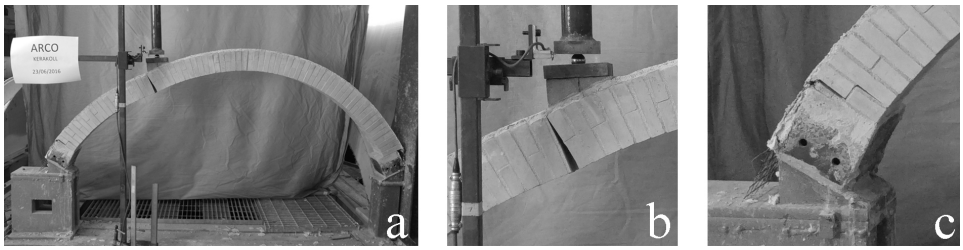

Figure 4. Basalt-FRLM-strengthened arch: (**a**) collapse mechanism; (**b**) opening of hinge 1; (**c**) opening of hinge 4.

Figure 5. Superficial cracks on lime matrix, where hinge 2 formed on the un-strengthened arch.

Figure 6 shows the load-displacement responses of the un-strengthened and Basalt-FRLM-strengthened arches. The displacement shown in this figure is the vertical displacement of the loaded cross-section. In Table 3, the contribution of Basalt-FRLM composite sheet can be noted in increasing the failure load (about 5 times) and kinematic ductility (about 20 times) with respect to the un-strengthened arches.

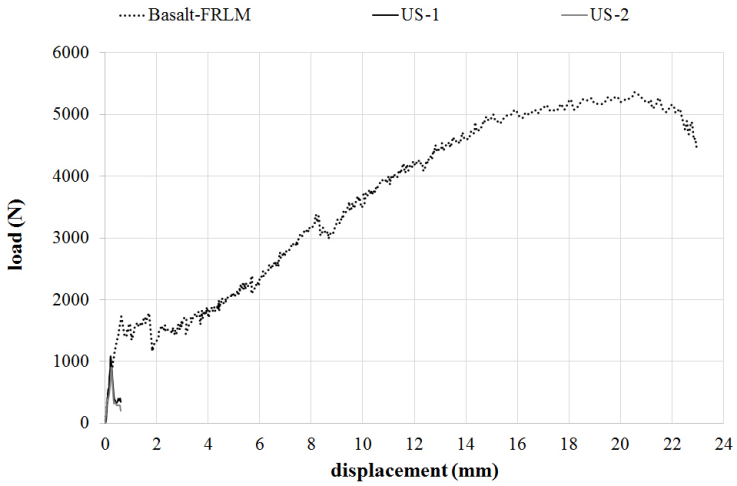

Figure 6. Load-displacement curves of un-strengthened and Basalt-FRLM-strengthened arch.

3.3. Comparison with Arches Strengthened with Cementitious and Polymeric Matrix Composites

The experimental results obtained on the arch model strengthened with Basalt-FRLM were compared with the experimental results of similar arch models strengthened with different composite materials (PBO-FRCM, CFRP) obtained in a previous step of this research [21,28]. The different composite materials had the same width, equal to the width of the arch extrados surface. Consequently, the fiber cross-sectional area was 3.2 mm^2, 1.4 mm^2 and 17 mm^2 in the case of Basalt-FRLM, PBO-FRCM, and CFRP composites, respectively. In Figure 7, the load-displacement curves of un-strengthened and

Basalt-FRLM-strengthened arches are compared with the load-displacement curves of PBO-FRCM- and CFRP-strengthened arches.

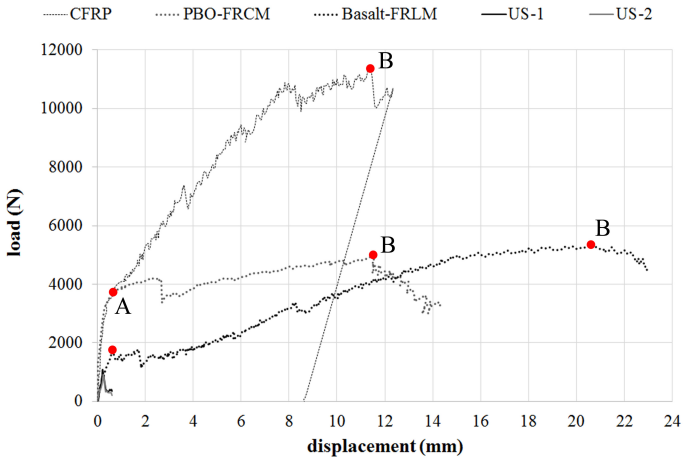

Figure 7. Load-displacement curves of un-strengthened and Basalt-FRLM-, PBO-FRCM-, and CFRP-strengthened arches.

The PBO-FRCM- and the Basalt-FRLM-strengthened arches exhibited a similar structural behavior. After the cracking of the loaded cross-section (Figure 9a), the PBO-FRCM cracked at the extrados of the cross-section where hinge 2 formed on the un-strengthened arch at a higher load than the Basalt-FRLM-strengthened arch (points A in Figure 7). This is probably related to the higher tensile strength of the cementitious matrix used for the PBO-FRCM material with respect to the natural lime mortar used for the Basalt-FRLM material (Table 2). Afterwards, the increase of the applied force is associated with an increase in the bending moment. Consequently, the thrust line crosses the intrados surface, as schematically shown in Figure 8.

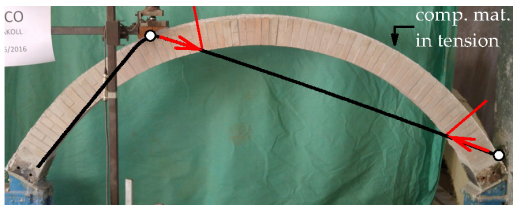

Figure 8. Schematic thrust line of the extrados-strengthened arches.

In this phase, the equilibrium condition requires a tensile force in the fibers (Figure 8). The increase of this tensile force after the cracking of the matrix and before the joint sliding at the right abutment (point B in Figure 7) is associated with a slip at the fiber-matrix interface, as evidenced by the crack pattern shown in Figures 5 and 9b. This allowed a good displacement capacity. It was observed that a greater number of cracks formed in the matrix of the PBO-FRCM composite than in the matrix of the Basalt-FRLM composite (Figures 5 and 9b). This indicates that higher interfacial shear stress acts at the PBO fiber-cement matrix interface than at the basalt fiber-lime mortar interface. The failure loads of the Basalt-FRLM- and PBO-FRCM-strengthened arches were similar, while the displacement capacity of the Basalt-FRLM-strengthened arch was higher than the displacement capacity of the PBO-FRCM-strengthened arch (Table 3). The different slope of the load-displacement responses of the PBO-FRCM- and Basalt-FRLM-strengthened arches is probably associated with different shapes of the bond-slip behavior of these composite materials; from the presented results, it can be argued that the fiber-matrix interface of the PBO-FRCM composite allows higher shear stress than the fiber-matrix interface of the Basalt-FRLM composite. Conversely, a non-zero shear stress is maintained up to

larger fiber-matrix slip in the case of the Basalt-FRLM composite than in the case of the PBO-FRCM composite. This statement needs to be confirmed by the results of shear bond tests to be performed on the Basalt-FRLM composite, while the bond behavior of the PBO-FRCM composite has been analyzed in several papers [14,28–32]. In References [16–18,25], it is shown that the failure load of strengthened arches can be analytically evaluated with the approach of the limit analysis. This requires the knowledge of the fiber debonding strain, i.e., the fibers strain associated with debonding at the fiber-matrix interface. The debonding strain of PBO-FRCM composites was experimentally determined by means of shear bond tests [14,28–32], while the debonding strain of the Basalt-FRLM material is not currently available. Therefore, the next step of this research work will involve the characterization of the Basalt-FRLM material in terms of bond behavior and the use of bond properties within the framework of the limit analysis to evaluate the collapse load of the Basalt-FRLM-strengthened arches.

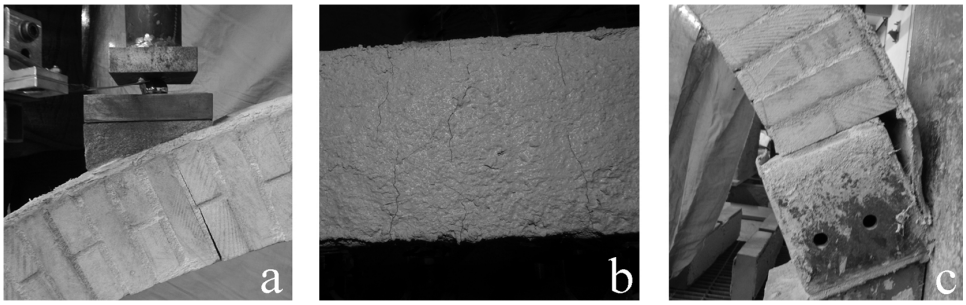

Figure 9. PBO-FRCM-strengthened arch: (**a**) hinge 1; (**b**) cracks in cementitious mortar matrix; (**c**) joint sliding at the right abutment [16].

The CFRP-strengthened arch exhibited brittle behavior. After the formation of the first hinge on the loaded cross-section and the cracking of the masonry where hinge 2 formed on the un-strengthened arch, the force in the fibers increased. This required lower interfacial slip than in the case of the PBO-FRCM and Basalt-FRLM composites, since the debonding phenomenon of FRP-masonry joints is associated with the formation of an interfacial crack within the supporting masonry [33–36]. The collapse was caused by the sudden shear sliding at the right abutment (Figure 10c). The collapse load of the CFRP-strengthened arch was roughly twice the collapse load of the PBO-FRCM- and Basalt-FRLM-strengthened arches. Conversely, the load-displacement response of the CFRP-strengthened arch showed lower displacement capacity than the PBO-FRCM- and Basalt-FRLM-strengthened arches.

Figure 10. CFRP-strengthened arch: (**a**) hinge 1; (**b**) opening of hinge 2; (**c**) joint sliding at the right abutment.

A comparison of the specific effectiveness of the strengthening of the composite materials considered in this experimental work can be performed considering the parameter Δf defined by Equation (1) (Table 3). Δf is representative of the strengthening effectiveness of the composite materials

even though the collapse of the arches was always associated with the shear force, since the composite materials bonded on the surface of an arch produces an increase in both the flexural and shear capacity of the strengthened cross-sections, as observed in References [17,25]. It can be observed that the increase of the collapse load associated with a unit fiber cross-section is higher for the PBO-FRCM and Basalt-FRLM composites with respect to the CFRP composite.

4. Conclusions

This paper concerns a preliminary study on the effectiveness of a composite material made of basalt textile and lime-based mortar matrix (Basalt-FRLM) for strengthening masonry structures. The structural behavior of arches strengthened at the extrados with Basalt-FRLM is experimentally evaluated. The results obtained highlight the effectiveness of the Basalt-FRLM composite; the maximum load and kinematic ductility results highly increased with respect to the un-strengthened arches (about 5 and about 20 times, respectively).

The Basalt-FRLM-strengthened arch exhibited similar failure load to and higher ductility than a similar arch strengthened with a composite material made of PBO fibers embedded in a cement-based matrix (PBO-FRCM). The different displacement capacity of the Basalt-FRLM- and PBO-FRCM-strengthened arches can be associated with the different fiber-matrix bond properties of these composite materials and to the lower elastic modulus of the basalt fibers with respect to carbon fibers. Furthermore, the Basalt-FRLM- and PBO-FRCM-strengthened arches exhibited a lower (roughly half) failure load than a similar arch strengthened with a carbon fiber reinforced polymer (CFRP) composite. This can be associated with the higher cross-sectional area of fibers in the CFRP composite than in the Basalt-FRCM composite (roughly 5 times) and PBO-FRCM composite (roughly 12 times).

The presented preliminary experimental results encourage further research on the use of the Basalt-FRCM composite for strengthening masonry structures, especially in terms of characterization of the basalt fibers-lime mortar bond properties, since the tests highlighted the excellent adhesion at the masonry-lime matrix interface.

The use of this type of composite is of interest to applications aimed at strengthening historical and monumental buildings where the historical compatibility with the substrate is strictly required. Moreover, the tested strengthening system responds to the increasing requirements of sustainable interventions.

Author Contributions: All the Authors contributes in the same way to the research.

Conflicts of Interest: The authors declare no conflict of interest.

References

1. Giresini, L.; Sassu, M. Horizontally restrained rocking blocks: evaluation of the role of boundary conditions with static and dynamic approaches. *Bull. Earthq. Eng.* **2016**, *15*, 385–410. [CrossRef]
2. Giresini, L.; Fragiacomo, M.; Sassu, M. Rocking analysis of masonry walls interacting with roofs. *Eng. Struct.* **2016**, *116*, 107–120. [CrossRef]
3. D'Ambrisi, A.; Feo, L.; Focacci, F. Masonry arches strengthened with composite unbonded tendons. *Compos. Struct.* **2013**, *98*, 323–329. [CrossRef]
4. Foraboschi, P. Resisting system and failure modes of masonry domes. *Eng. Fail. Anal.* **2014**, *44*, 315–337. [CrossRef]
5. Foraboschi, P.; Vanin, A. Non-linear static analysis of masonry buildings based on a strut-and-tie modeling. *Soil Dyn. Earthq. Eng.* **2013**, *55*, 44–58. [CrossRef]
6. Misseri, G.; Rovero, L. Parametric investigation on the dynamic behaviour of masonry pointed arches. *Arch. Appl. Mech.* **2017**, *87*, 385–404. [CrossRef]
7. Giresini, L. Energy-based method for identifying vulnerable macro-elements in historic masonry churches. *Bull. Earthq. Eng.* **2015**, *14*, 919–942. [CrossRef]
8. Andreini, M; De Falco, A.; Giresini, L.; Sassu, M. Structural damage in the cities of Reggiolo and Carpi after the earthquake on May 2012 in Emilia Romagna. *Bull. Earthq. Eng.* **2014**, *12*, 2445–2480. [CrossRef]

9. Andreini, M.; De Falco, A.; Giresini, L.; Sassu, M. Structural analysis and consolidation strategy of the historic Mediceo Aqueduct in Pisa (Italy). *Appl. Mech. Mater.* **2013**, *351–352*, 1354–1357. [CrossRef]
10. De Falco, A.; Giresini, L.; Sassu, M. Temporary preventive seismic reinforcements on historic churches: Numerical modeling of San Frediano in Pisa. *Appl. Mech. Mater.* **2013**, *352*, 1393–1396. [CrossRef]
11. Giresini, L.; Sassu, M. Tests Results and Simple Structural Analysis of the Main Lighthouse in the Harbor of Livorno (Italy). *Adv. Mater. Res.* **2014**, *834*, 1299–1303. [CrossRef]
12. Larrinaga, P.; Chastre, C.; San-José, J.T.; Garmendia, L. Non-linear analytical model of composites based on basalt textile reinforced mortar under uniaxial tension. *Compos. Part B Eng.* **2013**, *55*, 518–527. [CrossRef]
13. Prota, A.; Marcari, G.; Fabbrocino, G.; Manfredi, G.; Aldea, C. Experimental In-Plane Behavior of Tuff Masonry Strengthened with Cementitious Matrix–Grid Composites. *J. Compos. Constr.* **2006**, *10*, 223–233. [CrossRef]
14. Alecci, V.; De Stefano, M.; Luciano, R.; Rovero, L.; Stipo, G. Experimental Investigation on Bond Behavior of Cement-Matrix–Based Composites for Strengthening of Masonry Structures. *J. Compos. Constr.* **2015**, *20*, 04015041. [CrossRef]
15. Garmendia, L.; Larrinaga, P.; San-Mateos, R.; San-José, J.T. Strengthening masonry vaults with organic and inorganic composites: an experimental approach. *Mater. Des.* **2015**, *85*, 102–114. [CrossRef]
16. D'Ambrisi, A.; Focacci, F.; Luciano, R.; Alecci, V.; De Stefano, M. Carbon-FRCM materials for structural upgrade of masonry arch road bridges. *Compos. Part B Eng.* **2015**, *75*, 355–366. [CrossRef]
17. Alecci, V.; Focacci, F.; Rovero, L.; Stipo, G.; De Stefano, M. Extrados strengthening of brick masonry arches with PBO-FRCM composites: Experimental and analytical investigations. *Compos. Struct.* **2016**, *149*, 184–196. [CrossRef]
18. Alecci, V.; Misseri, G.; Rovero, L.; Stipo, G.; De Stefano, M.; Feo, L.; Luciano, R. Experimental investigation on masonry arches strengthened with PBO-FRCM composite. *Compos. Part B Eng.* **2016**, *100*, 228–239. [CrossRef]
19. Rovero, L.; Focacci, F.; Stipo, G. Structural behavior of arch models strengthened using FRP strips of different lengths. *J. Compos. Constr.* **2013**, *17*, 249–258. [CrossRef]
20. Briccoli Bati, S.; Rovero, L.; Tonietti, U. Strengthening of masonry arches with composite materials. *J. Compos. Mater.* **2007**, *11*, 33–42. [CrossRef]
21. Briccoli Bati, S.; Rovero, L. Towards a methodology for estimating strength and collapse mechanism in masonry arches strengthened with fibre reinforced polymer applied on external surfaces. *Mater. Struct.* **2008**, *41*, 1291–1306. [CrossRef]
22. Rotunno, T.; Rovero, L.; Tonietti, U.; Briccoli Bati, S. Experimental study of bond behavior of CFRP-to-brick joints. *J. Compos. Constr.* **2015**, *19*, 04014063. [CrossRef]
23. Alecci, V.; Briccoli Bati, S.; Ranocchiai, G. Study of brickwork columns confined with CFRP composite. *J. Compos. Constr.* **2009**, *13*, 179–187. [CrossRef]
24. De Felice, G.; De Santis, S.; Garmendia, L.; Ghiassi, B.; Larrinaga, P.; Lourenco, P.B.; Oliveira, D.V.; Paolacci, F.; Papanicolaou, C.G. Mortar-based systems for externally bonded strengthening of masonry. *Mater. Struct.* **2014**, *47*, 2021–2037. [CrossRef]
25. Alecci, V.; Focacci, F.; Rovero, L.; Stipo, G.; De Stefano, M. Intrados strengthening of brick masonry arches with different FRCM composites: experimental and analytical investigations. *Compos. Struct.* **2017**, in press. [CrossRef]
26. UNI EN 1015-11. *Methods of Test for Mortar for Masonry—Determination of Flexural and Compressive Strength of Hardened Mortar*; European Standard; BSI: London, UK, 2007.
27. UNI EN 772-1. *Methods of Test for Masonry Units—Determination of Compressive Strength*; European Standard: Milton Keynes, UK, 2011.
28. D'Ambrisi, A.; Feo, L.; Focacci, F. Bond-slip relations for PBO–FRCM materials externally bonded to concrete. *Compos. Part B Eng.* **2012**, *43*, 2938–2949. [CrossRef]
29. Caggegi, C.; Carozzi, F.G.; De Santis, S.; Fabbrocino, F.; Focacci, F.; Hojdys, Ł.; Lanoye, E.; Zuccarino, L. Experimental analysis on tensile and bond properties of PBO and aramid fabric reinforced cementitious matrix for strengthening masonry structures. *Compos Part B Eng.* **2017**, in press. [CrossRef]
30. Carloni, C.; D'Antino, T.; Sneed, L.; Pellegrino, C. Role of the matrix layers in the stress transfer mechanism of FRCM composites bonded to a concrete substrate. *J. Eng. Mech.* **2014**, *141*. [CrossRef]

31. D'Antino, T.; Carloni, C.; Sneed, L.H.; Pellegrino, C. Matrix-fiber bond behavior in PBO FRCM composites: A fracture mechanics approach. *Eng. Fract. Mech.* **2014**, *117*, 94–111. [CrossRef]
32. Focacci, F.; D'Antino, T.; Carloni, C.; Sneed, L.H.; Pellegrino, C. An indirect method to calibrate the interfacial cohesive material law for FRCM-concrete joints. *Mater. Des.* **2017**, *128*, 206–217. [CrossRef]
33. Focacci, F.; Carloni, C. Periodic variation of the transferable load at the FRP-masonry interface. *Compos. Struct.* **2015**, *129*, 90–100. [CrossRef]
34. Carloni, C.; Focacci, F. FRP-masonry interfacial debonding: An energy balance approach to determine the influence of the mortar joints. *Eur. J. Mech.—A/Solids* **2016**, *55*, 122–133. [CrossRef]
35. Malena, M.; Focacci, F.; Carloni, C.; De Felice, G. The effect of the shape of the cohesive material law on the stress transfer at the FRP-masonry interface. *Compos. Part B Eng.* **2017**, *110*, 368–380. [CrossRef]
36. Foraboschi, P. Effectiveness of novel methods to increase the FRP-masonry bond capacity. *Compos. Part B Eng.* **2016**, *107*, 214–232. [CrossRef]